Optical manipulation of plasmonic nanoparticles, bubble formation and patterning of SERS aggregates

2010 Nanotechnology 21 105304

(http://iopscience.iop.org/0957-4484/21/10/105304)

Nanotechnology **21** (2010) 105304 (5pp) doi:10.1088/0957-4484/21/10/105304

Optical manipulation of plasmonic nanoparticles, bubble formation and patterning of SERS aggregates

Zuwei Liu[1], **Wei Hsuan Hung**[2], **Mehmet Aykol**[3], **David Valley**[4] and **Stephen B Cronin**[1,3,4]

[1] Department of Physics, University of Southern California, Los Angeles, CA 90089, USA
[2] Department of Materials Science, University of Southern California, Los Angeles, CA 90089, USA
[3] Department of Electrical Engineering, University of Southern California, Los Angeles, CA 90089, USA
[4] Department of Chemistry, University of Southern California, Los Angeles, CA 90089, USA

E-mail: scronin@usc.edu

Received 16 October 2009, in final form 24 January 2010
Published 16 February 2010
Online at stacks.iop.org/Nano/21/105304

Abstract

We present an optical method for patterning SERS (surface-enhanced Raman spectroscopy)—enhancing aggregates of gold nanoparticles, using a focused laser beam to optically trap the nanoparticles in suspension. At high laser powers, heat generated from the plasmonic excitation causes boiling of the aqueous suspension and the formation of gaseous bubbles of water vapor. By measuring the Raman peak of the hydroxyl bond of water, the temperature in the laser spot during the aggregation can be determined *in situ*. The hydrophilic nanoparticles are found to aggregate at the liquid–vapor interface. By allowing the suspension to dry, a ring of gold nanoparticles is deposited on the substrate, producing a highly SERS-active region. These aggregates are studied using optical microscopy, scanning electron microscopy and micro-Raman spectroscopy.

(Some figures in this article are in colour only in the electronic version)

1. Introduction

The irradiation of plasmonic nanoparticles has become an important area of research with applications in chemical sensing [1, 2], non-invasive cancer treatment therapy [3], and even carbon nanotube and nanowire growth [4, 5]. Many techniques for depositing plasmonic nanoparticles have been explored [6–12], including DNA linking of nanoparticles [13], block copolymer lithography [10], two-phase-mediated functionalization [14] and electron beam lithography [7]. The plasmonic response of metal nanoparticles has also been extensively studied theoretically [15–17]. These calculations show that the plasmonic resonance increases asymptotically as the particles are brought closer together. The calculations of Schatz *et al*, using an interacting dipole model, have shown the plasmonic field enhancement to be 10^3 times stronger between two nearly touching nanoparticles [15]. Finite-difference time domain (FDTD) simulations have also shown that coupled nanoparticles produce large electric field enhancements of the order of 10^3 and surface-enhanced Raman spectroscopy (SERS) enhancement factors up to 10^{12} [16, 17]. While block copolymer lithography and electron beam lithography produce very uniform arrays of nanoparticles, they cannot produce the small separations needed for immense plasmonic excitation. Here, we present a method for producing large aggregates (5–10 μm in size) of nanoparticles (20 nm in diameter) that are strongly plasmonic and, consequently, strongly SERS-active.

Since the discovery of optical trapping, 30 years ago [18], optical tweezers have become a powerful tool in biophysics. Currently, optical tweezers are commonly used to trap and manipulate cells [19] and to sort micron-sized dielectric

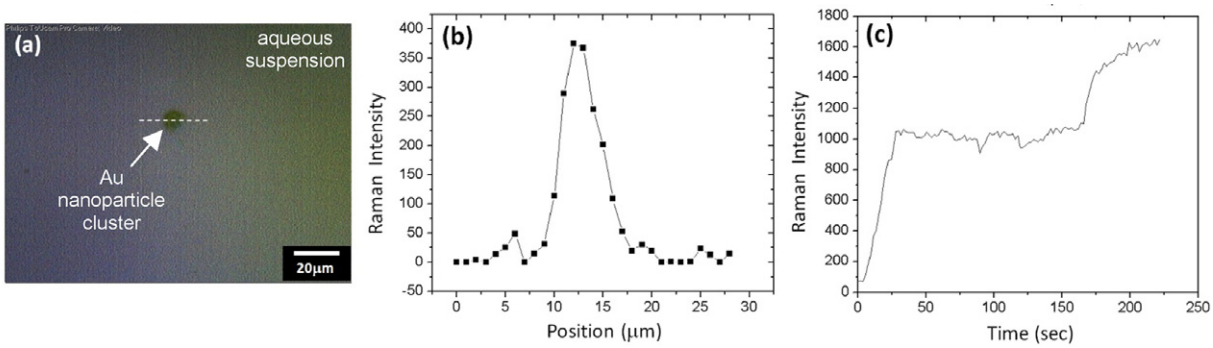

Figure 1. (a) Optical microscope image, (b) spatial profile and (c) time evolution of the Raman intensity of a gold nanoparticle aggregate induced by laser irradiation.

spheres [20]. The concept of optical trapping has also been extended to manipulate objects on the nanoscale and even the single-atom scale [21, 22].

2. Experiment

In this work, a 532 nm 5 W Spectra Physics solid state laser is collimated and focused through a Leica *DM*LM microscope with a 50× long-working-distance objective lens with NA = 0.5. The beam diameter was measured using the knife-edge method [23] to be 1.25 μm. Microfluidic channels are etched in silicon by deep reactive ion etching (DRIE) with typical channel dimensions of 100 μm wide by 50 μm deep. The channels are sealed with a glass coverslip using anodic bonding, which forms a permanent bond at the glass–Si interface [24]. A colloidal suspension of 20 nm diameter gold nanoparticles (British-Biocell, Cardiff, UK) is pumped through the microchannels and irradiated with the focused laser spot. The resonance wavelength of the gold colloidal particle suspension occurs at approximately 520 nm, which is close to the wavelength of laser excitation. After allowing the sample to dry, this aggregated structure is studied by scanning electron microscopy (SEM) and micro-Raman spectroscopy.

3. Results and discussion

Figure 1(a) shows an optical microscope image of a suspension of colloidal gold nanoparticles after a 220 s laser exposure at a power of 30 mW μm^{-2}. Here, the suspension is simply confined between a silicon wafer and a glass coverslip. The image shows a dark spot approximately 5 μm in size at the location of the focused laser spot. This dark spot indicates an aggregate of gold nanoparticles that were optically trapped in the aqueous suspension by the large electric field gradients near the tightly focused laser beam. This aggregate was observed to disperse back into the suspension several minutes after the laser was turned off, indicating that the nanoparticles in the aggregate are only weakly bound. We can rule out evaporation of the aqueous suspension as a possible cause for this aggregation on the basis that the suspension is confined between a glass coverslip and an underlying silicon substrate. Therefore, there is no liquid–gas interface from which the suspension can evaporate. The basic principles of gold nanoparticle aggregation can be understand from the theory of optical tweezers [25]. In the nanoscale size regime of the 20 nm nanoparticles, which is much smaller than the wavelength of the light (532 nm), the force created by the light is proportional to the intensity gradient, $F \propto \nabla I$. The tightly focused laser beam creates a large electric field intensity gradient in the Au nanoparticle suspension. The gradient creates a force on the nanoparticles in suspension, pushing them towards the focal point, thus causing aggregation. By measuring the Raman signal from the stabilizer citrate of the AuNP suspension, a spatial mapping of the Raman intensity profile across this dark spot (indicated by the dashed white line in figure 1(a)) can be seen in figure 1(b). This profile shows a region of approximately 5 μm exhibiting an enhanced Raman intensity. Figure 1(c) shows the Raman intensity measured during a 220 s laser exposure. Initially, we see a linear increase in the Raman intensity with time, as the nanoparticles aggregate. After 40 s, the Raman intensity remains constant, which we attribute to the depletion of all the nanoparticles in the local vicinity that have been sequestered into the aggregate. As further evidence of this, we find that, once an aggregate is formed, another aggregate cannot be formed in close proximity to the first aggregate, which has taken up all of the nearby gold nanoparticles. After the nanoparticles from remote regions have had a chance to diffuse into the region of the focused laser spot (>160 s), the SERS intensity is observed to increase again.

Figure 2 shows the optical microscope images of a silicon microchannel containing the colloidal nanoparticle suspension before and after 30 s and 2 min exposures, again at a laser power of 30 mW μm^{-2}. In figures 2(b) and (c), a bubble of water vapor is seen to grow from 15 to 60 μm in diameter, respectively. The dark ring surrounding the bubble corresponds to the optical absorption of the gold nanoparticles, which aggregate at the water–vapor interface. When the laser is turned off, the bubble shrinks during the first few minutes as the temperature decreases, as shown in figure 2(d). The bubble then remains constant in size once the temperature equilibrates with room temperature. From the ideal gas law and the change in volume of the bubble, the initial temperature of the water vapor can be estimated to be around 400 °C immediately after the laser is turned off. To exclude the possibility of laser heating of the underlying substrate, a control experiment

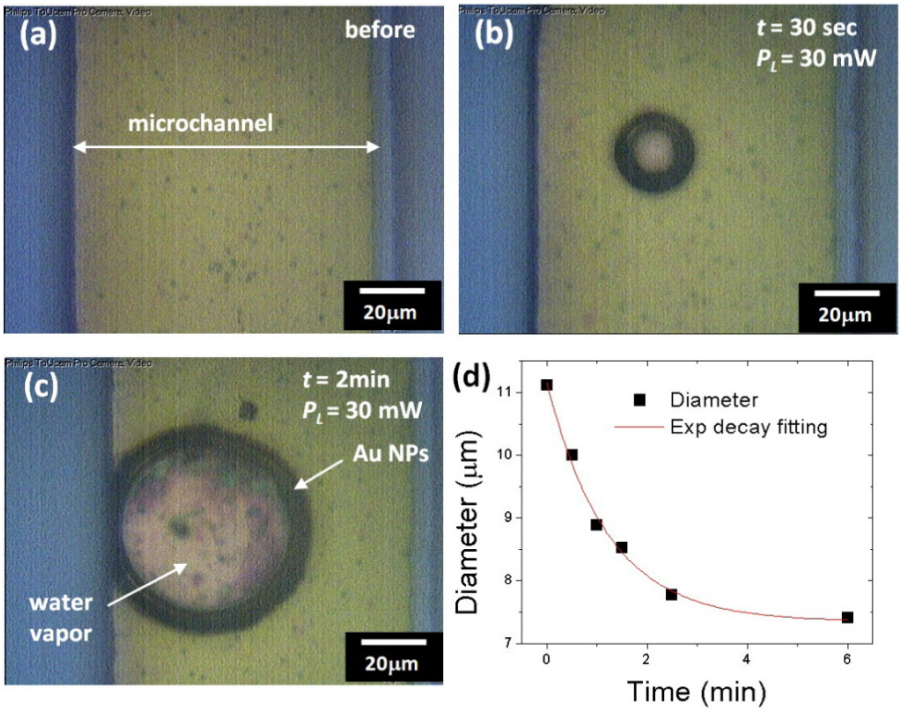

Figure 2. ((a)–(c)) Optical microscope images of Au nanoparticle aggregation and bubble formation induced by laser irradiation. (d) Bubble diameter plotted as a function of time after the laser is turned off.

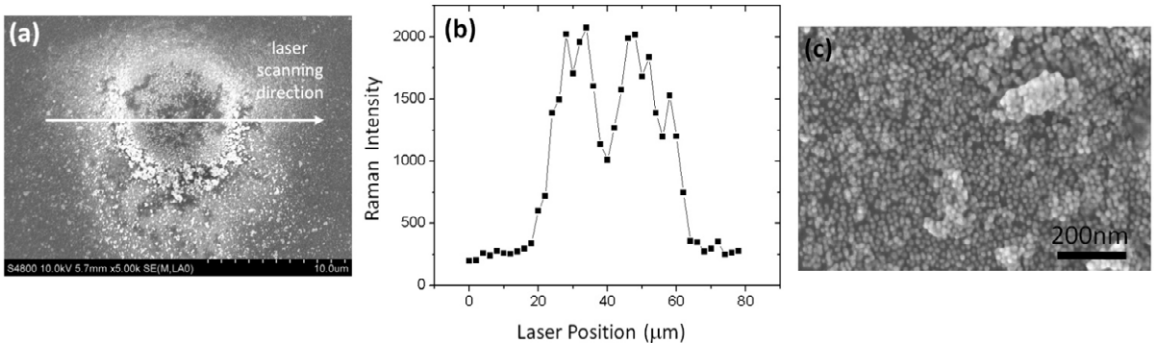

Figure 3. (a) SEM image and (b) Raman intensity profile across a nanoparticle aggregate deposited on the substrate. (c) High magnification SEM image of the nanoparticle aggregate region.

was performed without gold nanoparticles in the suspension, which showed no bubble formation even for laser exposures of 10 min.

The small dimensions of the microchannel-confined suspension provide an additional experimental parameter for controlling nanoparticle heating and bubble formation. In fact, we do not observe any bubble formation in the nanoparticle suspension confined by a glass coverslip. The reduced heat capacity in the microchannels, however, enables rapid heating of the suspension and bubble formation. In addition, the bubble formation dynamics provide a new way to study the heat flow from plasmonic nanoparticles to their surrounding aqueous suspension.

As mentioned above, the nanoparticles disperse uniformly back into the suspension after the laser is turned off. However, if the suspension is allowed to dry with the laser on, then the nanoparticle aggregate is deposited on the substrate. This can be seen in figure 3, which shows an SEM image of one such deposition. The ring-shape nature of this deposition is apparent from these images. From high resolution SEM images (figure 3(c)), we find the nanoparticle density to be quite high in the region of the ring and significantly lower in the center and outside the ring. In order to quantify the SERS enhancement of these Au nanoparticle depositions, we deposit ATP (aminothiophenol) dye molecules. We then perform a spatial line scan of the Raman intensity across the ring, as shown in figure 3(b). Here, a maximum Raman intensity occurs on the ring, rather than in the center or outside the ring. From the SEM images, we determine the relative nanoparticle densities outside, on and inside the ring to be roughly 1:10:5, which is consistent with the Raman intensity ratios observed in figure 3(b). If a 5 nm thick film of Au is

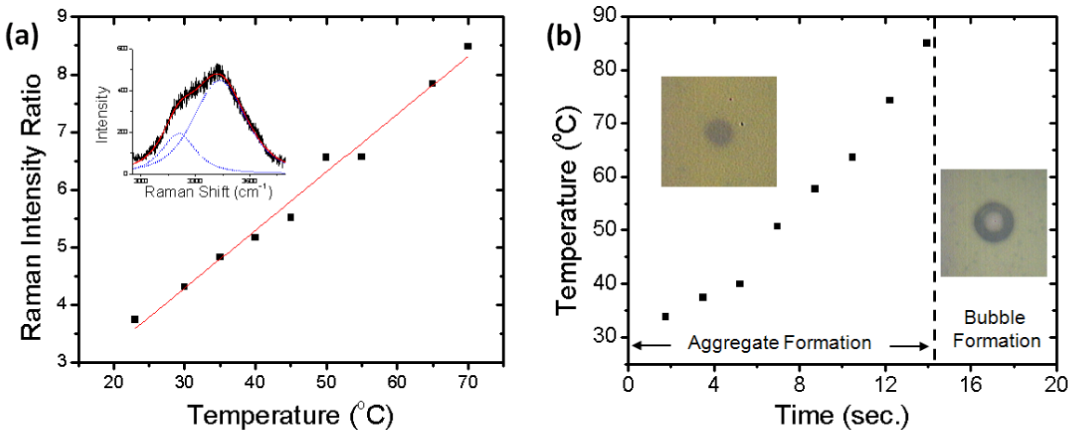

Figure 4. (a) Temperature calibration of the hydroxyl stretching mode Raman intensity ratio. (b) Temperature plotted as a function of laser exposure time, indicating nanoparticle aggregation and bubble formation.

deposited on the substrate, the nanoparticle aggregation and bubble formation is found to occur much faster than on a blank silicon substrate. The reason for this enhancement is that the pre-deposited Au film, which is known to be strongly plasmonic [26], produces a much stronger electric field than the nanoparticles in suspension alone. This technique provides an easy way to manipulate the position, temperature and electric fields of plasmonic nanoparticles. By using various optical fields, different patterns of plasmonic nanoparticles can be created in suspension or patterned on the substrate. From our Raman measurements, it is difficult to quantify the SERS enhancement factor because the number of molecules in the focal volume of the laser spot is unknown. By comparing the Raman intensities of the citrate peak of the Au nanoparticle aggregates with that of the non-aggregated nanoparticles in suspension, we estimate a SERS enhancement factor of 10^5 beyond the non-aggregated nanoparticles in suspension.

It is well known that the shape of the stretching band of the hydroxyl group in liquid water, which lies between 3100 and 3700 cm^{-1}, is very sensitive to temperature [27]. By fitting this band to two peaks, the ratio of their intensities varies linearly with temperature [28]. Figure 4(a) shows the calibration of this intensity ratio taken in a temperature-controlled stage. The ratio varies from a value of 3.7–8.5 between 23 and 70 °C, with a linear fit of $I_2/I_1 = 0.100\,64T + 1.273$. Figure 4(b) shows the temperature of the aqueous solution of Au nanoparticles measured in this way during a 21 s laser exposure. During the first 14 s, the temperature increases monotonically from 33 to 85 °C. During this time a dark spot indicating aggregate formation can be seen in the optical microscope image, as shown in the inset. After 15 s of laser exposure, bubble formation can be seen in the optical microscope image (see the inset). Once the bubble is formed, this stretching mode can no longer be observed. Nevertheless, this bubble formation coincides nicely with the boiling point of the aqueous solution (100 °C). We should mention that the boiling time for this solution is significantly shorter than that shown in figure 1, because of the small size and heat capacity in the microchannel.

4. Conclusion

In conclusion, we present an optical method for patterning SERS-enhancing aggregates of gold nanoparticles, using a focused laser spot to optically trap gold nanoparticles in suspension. Heat generated due to the plasmonic excitation causes boiling of the aqueous suspension and the formation of water vapor bubbles. The hydrophilic nanoparticles aggregate at the liquid–vapor interface, while the gas bubbles grow in size during the course of laser irradiation. When the laser is turned off, the bubbles shrink in size until they equilibrate with room temperature. By allowing the suspension to dry, a ring of gold nanoparticles is deposited on the substrate that is highly SERS-active. From spatial mapping of the Raman intensity, a clear SERS enhancement factor is seen in a 5 μm cluster.

Acknowledgments

This research was supported in part by ONR Award no. N00014-08-1-0132 and AFOSR Award no. FA9550-08-1-0019.

References

[1] Schultz S G, Janikczachor M and van Duyne R P 1981 Surface enhanced Raman spectroscopy—a reexamination of the role of surface-roughness and electrochemical anodization *Surf. Sci.* **104** 419–34

[2] Kneipp K, Wang Y, Kneipp H, Perelman L T, Itzkan I, Dasari R and Feld M S 1997 Single molecule detection using surface-enhanced Raman scattering (SERS) *Phys. Rev. Lett.* **78** 1667–70

[3] Pissuwan D, Valenzuela S M and Cortie M B 2006 Therapeutic possibilities of plasmonically heated gold nanoparticles *Trends Biotechnol.* **24** 62–7

[4] Hung W H, Hsu I-K, Bushmaker A, Kumar R and Cronin S B 2008 Laser directed growth of carbon-based nanostructures by plasmon resonant chemical vapor deposition *Nano Lett.* **8** 3278

[5] Boyd D A, Greengard L, Brongersma M, El-Naggar M Y and Goodwin D G 2006 Plasmon-assisted chemical vapor deposition *Nano Lett.* **6** 2592–7

[6] Hicks E M, Zhang X Y, Zou S L, Lyandres O, Spears K G, Schatz G C and Van Duyne R P 2005 Plasmonic properties of film over nanowell surfaces fabricated by nanosphere lithography *J. Phys. Chem.* B **109** 22351–8
[7] Atay T, Song J H and Nurmikko A V 2004 Strongly interacting plasmon nanoparticle pairs: from dipole–dipole interaction to conductively coupled regime *Nano Lett.* **4** 1627–31
[8] Van Duyne R P, Hulteen J C and Treichel D A 1993 Atomic-force microscopy and surface-enhanced Raman spectroscopy. I. Ag island films over polymer nanosphere surfaces supported on glass *J. Chem. Phys.* **99** 2101–15
[9] Kumar R, Zhou H and Cronin S B 2007 Surface-enhanced Raman spectroscopy and correlated scanning electron microscopy of individual carbon nanotubes *Appl. Phys. Lett.* **91** 223105
[10] Jaramillo T F, Baeck S H, Cuenya B R and McFarland E W 2003 Catalytic activity of supported Au nanoparticles deposited from block copolymer micelles *J. Am. Chem. Soc.* **125** 7148–9
[11] Meltzer S, Resch R, Koel B E, Thompson M E, Madhukar A, Requicha A A G and Will P 2001 Fabrication of nanostructures by hydroxylamine seeding of gold nanoparticle templates *Langmuir* **17** 1713–8
[12] Markel V A, Shalaev V M, Zhang P, Huynh W, Tay L, Haslett T L and Moskovits M 1999 Near-field optical spectroscopy of individual surface-plasmon modes in colloid clusters *Phys. Rev.* B **59** 10903–9
[13] Park S Y, Lytton-Jean A K R, Lee B, Weigand S, Schatz G C and Mirkin C A 2008 DNA-programmable nanoparticle crystallization *Nature* **451** 553–6
[14] Yim T J, Wang Y and Zhang X 2008 Synthesis of a gold nanoparticle dimer plasmonic resonator through two-phase-mediated functionalization *Nanotechnology* **19** 435605
[15] Zou S L and Schatz G C 2005 Silver nanoparticle array structures that produce giant enhancements in electromagnetic fields *Chem. Phys. Lett.* **403** 62–7
[16] Oubre C and Nordlander P 2005 Finite-difference time-domain studies of the optical properties of nanoshell dimers *J. Phys. Chem.* B **109** 10042
[17] Nordlander P, Oubre C, Prodan E, Li K and Stockman M I 2004 Plasmon hybridization in nanoparticle dimers *Nano Lett.* **5** 899
[18] Ashkin A 1970 Acceleration and trapping of particles by radiation pressure *Phys. Rev. Lett.* **24** 156
[19] Ashkin A and Dziedzic J M 1987 Optical trapping and manipulation of viruses and bacteria *Science* **235** 1517–20
[20] Čižmár T, Šiler M, Šerý M and Zemánek P 2006 Optical sorting and detection of submicrometer objects in a motional standing wave *Phys. Rev.* B **74** 035105
[21] Svoboda K and Block S M 1994 Optical trapping of metallic Rayleigh particles *Opt. Lett.* **19** 930
[22] Tong L, Righini M, Gonzalez M U, Quidant R and Kall M 2009 Optical aggregation of metal nanoparticles in a microfluidic channel for surface-enhanced Raman scattering analysis *Lab Chip* **9** 193
[23] Cohen D K, Little B and Luecke F S 1984 Techniques for measuring 1 μm diameter Gaussian beams *Appl. Opt.* **23** 637–40
[24] Knowles K M and van Helvoort A T J 2006 Anodic bonding *Int. Mater. Rev.* **51** 273–311
[25] Grier D G 2003 A revolution in optical manipulation *Nature* **424** 810–6
[26] Kumar R, Zhou H and Cronin S B 2007 Surface-enhanced Raman spectroscopy and correlated scanning electron microscopy of individual carbon nanotubes *Appl. Phys. Lett.* **91** 223105
[27] Kargovsky A V 2006 On temperature dependence of the valence band in the Raman spectrum of liquid water *Laser Phys. Lett.* **3** 567–72
[28] Pikov V and Siegel P H 2008 Remote temperature monitoring of cells exposed to millimeter-wave radiation using microscopic Raman spectroscopy *Eng. Med. Biol.* at press